Small-Signal Modeling of I^2 Average Current Mode Control

Siyu He, *Student Member, IEEE*, John Y. Hung, *Fellow, IEEE*, and R. M. Nelms, *Fellow, IEEE*

***Abstract*—I^2 average current mode control is a promising control technique featuring fast dynamic response, cycle-by-cycle current limiting and accurate current control. It can be treated as peak current mode control with no peak-to-average error. By combining direct current feedback and average current feedback, I^2 average current mode control is a three-loop control system. Since it is a new control technique proposed in 2013, few papers exist which discuss the small-signal model for this control method. In this paper, a small-signal model for constant frequency I^2 average current mode control is proposed which successfully predicts the subharmonics oscillation when the duty cycle is close to or greater than 0.5. The characteristics of I^2 average current mode control are also compared with average current mode control and peak current mode control to show its advantages.**

***Index Terms*—Average current mode control (ACM), dc–dc converters, frequency response measurement, small-signal modeling.**

I. Introduction

CURRENT mode control for switch-mode power supplies has been studied for over three decades [1], [2]. The first proposed current control technique, peak current mode control (PCM), has been widely used in the low-to-medium power applications due to simplification of the control loop design, cycle-by-cycle current limiting, and prevention of transformer/inductor flux imbalance [3], [4]. Since the inner current loop determines the duty ratio for the active switch in the converter by using the peak value of the inductor current, the peak-to-average error makes PCM lose the ability to control the current precisely [5]. For applications where a current source is preferred, like an LED driver or a battery charger, PCM can barely have zero dc error in the inductor current. As a result, average current mode control (ACM) is used instead of PCM [6], [7]. Compared to PCM, a PI controller is utilized in the current loop to provide infinite dc gain. For ACM, a high frequency pole in the current loop controller makes the loop less robust and a pure PI compensator is recommended [8]. Thus, the ripple in the inductor current still appears on the output of the current loop compensator while retaining the shape of the original waveform. However, the PI controller narrows the bandwidth of the current loop slowing the transient response.

Engineers have attempted to use PCM and ACM simultaneously to obtain both fast dynamic performance and zero DC error. A new control technique based on this same idea was proposed in the 2013 [9] and is referred to as I^2 ACM control. The current loop uses the inductor current signal twice—an average signal calculated by a PI controller and the peak/valley signal without modification. These two signals determine the duty ratio of the active switch in the same manner as the voltage signals in V^2 control [10]. As shown by the red line in Fig. 1, the PI compensator produces the average current signal, which is compared to the current command. This loop with the PI compensator is designated as a slow loop, which makes the inductor work as a current source with zero dc error. The peak/valley current signal, shown by the blue line in Fig. 1, is directly fed back without delay. As a result, this loop is referred to as the fast loop, which ensures current limiting and fast dynamic performance. In constant frequency operation, the switch turns on at the beginning of every switching cycle, it turns off at the moment when the fast loop waveform reaches the slow loop waveform as shown in Fig. 2. Therefore, there is no external saw-tooth signal needed for pulse width modulation (PWM) modulation as that needed in ACM and voltage mode control. The green line is the outer voltage loop, which produces the current command to keep the output voltage constant.

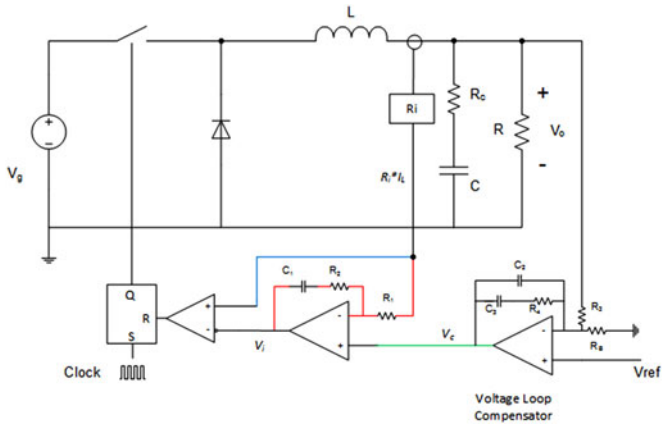

Fig. 1. I^2 ACM.

Compared to the traditional current mode control, I^2 ACM control has three loops instead of two. The modeling of this technique is more complicated than the other current control methods. The authors of [9] used describing functions to derive the *s*-domain transfer function by integrating several circuits into a functional block. This procedure yields little insight into the current loop and the cause of subharmonic oscillations. In this paper, I^2 ACM control is analyzed in detail, and a small-signal model is proposed that is applicable for constant frequency operation. An explanation for the subharmonic oscillations is

Manuscript received February 5, 2015; revised April 17, 2015 and June 17, 2015; accepted July 17, 2015. Date of publication July 22, 2015; date of current version December 10, 2015. Recommended for publication by Associate Editor J. A. Cobos.

The authors are with the Department of Electrical and Computer Engineering, Auburn University, Auburn, AL 36849 USA (e-mail: SZH0040@auburn.edu; hungjoh@auburn.edu; nelmsrm@auburn.edu).

Color versions of one or more of the figures in this paper are available online at http://ieeexplore.ieee.org.

Digital Object Identifier 10.1109/TPEL.2015.2459912

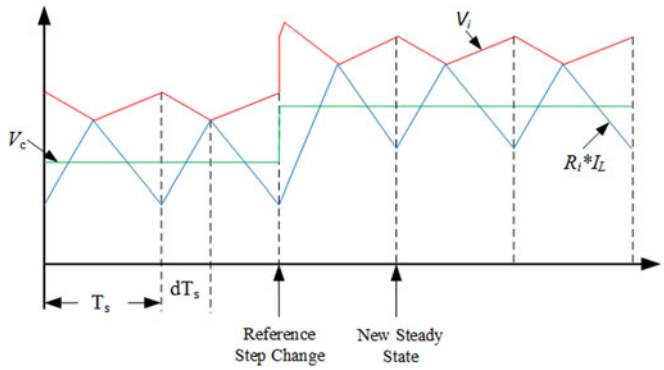

Fig. 2. Current waveform for I^2 ACM control.

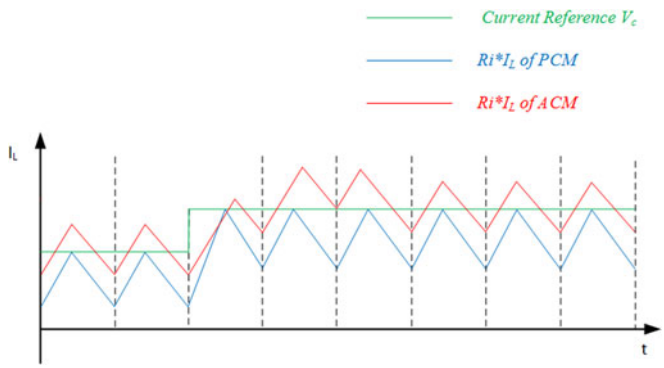

Fig. 3. Current waveforms for PCM and ACM control.

developed using this model, which is verified by both simulation and experiment.

II. I^2 ACM Control

A constant frequency trailing edge-modulated I^2 average current mode-controlled buck converter is shown in Fig. 1. The inductor current is used twice to determine the switch duty ratio. The waveforms for the current loop are shown in Fig. 2. A pure PI controller is utilized, because its delay is much less than that of an integral lead-lag compensator. A reference change in the current propagates through the current loop controller and appears at the output V_i. The switch is turned on at the beginning of each cycle by the system clock and turns off at the instance the inductor current reaches V_i; therefore, the inductor current works as the modulator slope. In I^2 control, both the average value and peak value of the inductor current are utilized, which in turn provides accurate current control and cycle-by-cycle adjustment. As a result, I^2 ACM control can be treated as a mixture of PCM and ACM, which combines the advantages of the two control methods. To illustrate the characteristics of I^2 ACM control, the current waveforms for ACM and PCM are also shown in Fig. 3. By comparing the current waveforms in Figs. 2 and 3, traditional PCM and ACM have a tradeoff between speed and accuracy; however, I^2 ACM control maintains both fast dynamics and precise control.

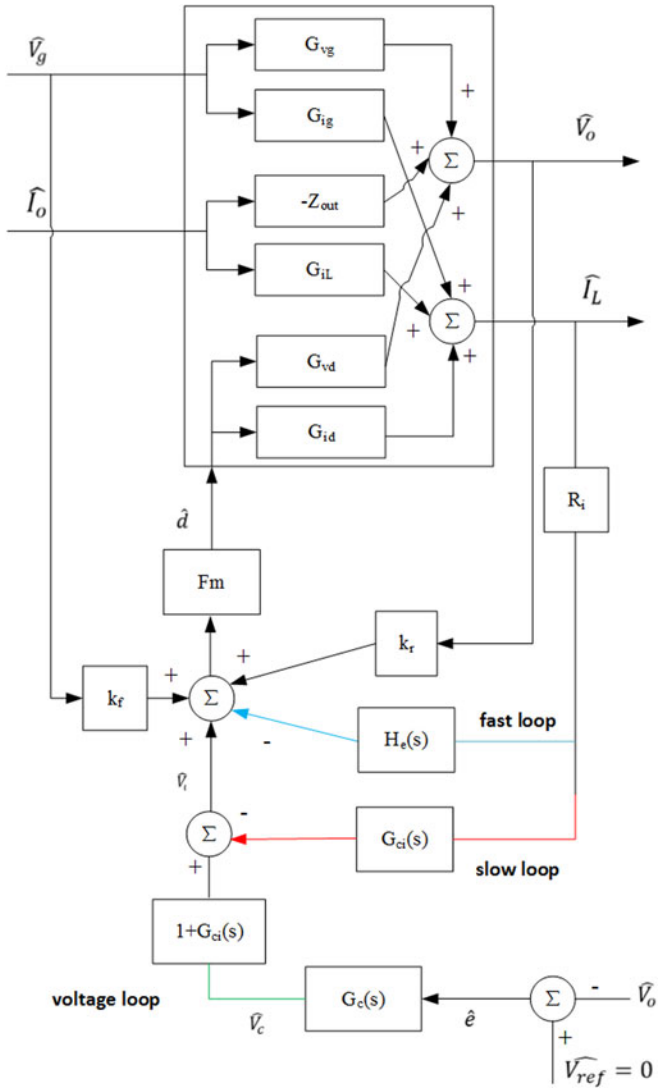

Fig. 4. Small-signal model for I^2 ACM control.

III. Small-Signal Modeling

The circuit in Fig. 1 has three loops: a fast loop shown in blue line, a slow loop in red, and a voltage loop in green. In the analysis of the current loop, assume that the voltage loop is open. Ignoring the slow loop, the fast loop forms a control circuit that looks like that of PCM. By ignoring the fast loop, the slow loop is similar to ACM. Hence, I^2 ACM control can be taken as a control system with a current loop having a PCM circuit and an ACM circuit in parallel. The corresponding small-signal model is shown in Fig. 4, where G_{vd} is the duty cycle-to-output voltage transfer function [11], G_{id} is duty cycle-to-inductor current transfer function [12], G_{vg} is the input-to-output voltage transfer function, G_{ig} is the input-to-inductor current transfer function, $Z_{\rm out}$ is the output impedance of the power stage, G_{iL} is the transfer function from load current to inductor current, G_o is the compensator in the voltage loop, G_{ci} is the controller in the current loop, F_m is the modulator gain, R_i is the current sense resistor, H_e is the sampling gain, $V_{\rm ref}$ is the voltage reference, V_o

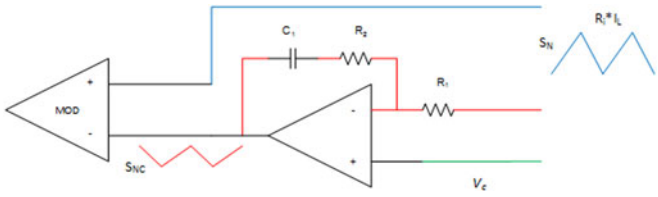

Fig. 5. Current compensator and modulator.

is the output voltage, I_L is the inductor current, V_c is the current reference, V_i is the slow loop current compensator output, and d is the duty cycle applied to the switch. Normally, the feedforward gains k_f and k_r are small, have little effect on the current loop gain, and can be ignored in the early stage analysis.

Although there is an integrator in the current loop, the gain $(1 + G_{ci}(s))$ in the forward path transmits the change in the current reference without delay. The current ripple, which is utilized instead of an external saw-tooth signal to determine the duty ratio, contains the circuit operating information and makes the transient response faster.

It should be noted that the modulator gain F_m in this control technique is different from those of PCM and ACM; an expression for this gain will be derived later. The gains k_r and k_f from the input and output voltage to inductor current are typically found in PCM and ACM models; however, they are also different from those utilized in the traditional control methods due to the two current loops.

A. Modulator Gain

For the current compensator in Fig. 5, the s-domain transfer function is

$$G_{ci}(s) = \frac{k_{ci} \cdot (1 + s/\omega_{zci})}{s} \tag{1}$$

where $\omega_{zci} = \frac{1}{C_1 \cdot R_2}$ and $k_{ci} = \frac{1}{C_1 \cdot R_1}$.

The phase delay introduced by (1) is

$$\text{delay} = \tan^{-1}(2\pi f_s C_1 R_2) - 90^\circ \tag{2}$$

where f_s is the frequency of the signal being processed. The negative value in (2) indicates that the output of the current compensator is lagging the input. Generally, capacitor C_1 and resistor R_2 produce a zero located below the resonant frequency of the power stage; thus, the first term in (2) is close to 90°. Taking the inverted input into consideration, the current compensator output is similar to the inverted inductor current. Assume that the input signal (the inductor current) has a rising slope of S_n, the corresponding compensated output signal has the falling slope S_{nc} at the switch turn-on instant and can be calculated as follows.

The s-domain transfer function for the inductor current while the switch is turning on, $I_L(s) = \frac{S_n}{s^2}$, the output of the current compensator is expressed as

$$V_i(s) = -G_{ci}(s) \cdot I_L(s) = -S_n \cdot k_{ci} \cdot \left(\frac{1}{\omega_{zci} \cdot s^2} + \frac{1}{s^3}\right)$$

where the minus sign is due to the current feeding back to the inverted input of the current compensator. By using the inverse

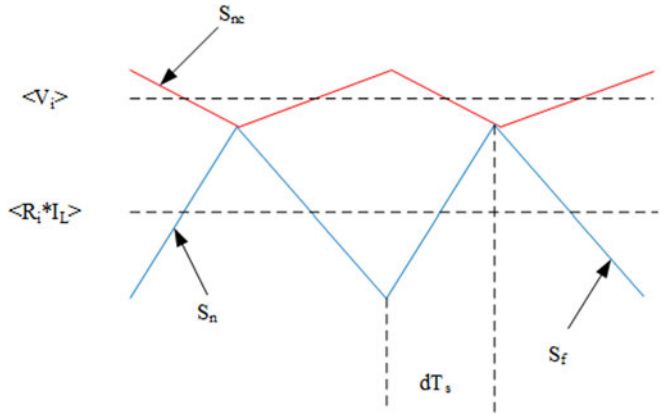

Fig. 6. Current waveforms for modulator.

Laplace transformation, the output can be represented in the time domain

$$V_i(t) = -S_n \cdot k_{ci} \cdot \left(\frac{t}{\omega_{zci}} + \frac{t^2}{2}\right).$$

Taking the derivative of the previous equation and evaluating it at time $t = DT_s$ yields S_{nc}

$$S_{nc} = -S_n \cdot k_{ci}(DT_s + 1/\omega_{zci}). \tag{3}$$

It can be noticed from (3) that S_{nc} varies with the duty ratio and the current loop compensator design; therefore, the overall modulator gain varies with operating point.

With the slope of the inductor current and the current compensator output, the waveforms which describe the modulation are shown in Fig. 6. The variables $\langle V_i \rangle$ and $\langle R_i^* I_L \rangle$ indicate the average value in a cycle, which are marked by dashed lines. Since the angle calculated from (2) is close to zero in most cases, the delay introduced by the PI controller can be safely approximated as 180°. Therefore, (4) is satisfied during steady-state operation. Since the waveforms for both the fast loop and slow loop are changing in a cycle, the absolute slope for modulation is related to the difference between the slopes of the two current waveforms

$$\langle V_i \rangle = \langle R_i \cdot I_L \rangle + \frac{1}{2} DT_s(S_n - S_{nc}). \tag{4}$$

Perturb the inductor current while keeping the other parameters fixed to obtain the modulator gain, F_{m1}, of the fast loop [12]

$$F_{m1} = \frac{\hat{d}}{\langle R_i \widehat{I_L} \rangle} = -\frac{2}{(S_n - S_{nc}) \cdot T_s}. \tag{5}$$

The similar methodology can be used to derive the modulator gain, F_{m2}, in the slow loop

$$F_{m2} = \frac{\hat{d}}{\langle \widehat{V_i} \rangle} = \frac{2}{(S_n - S_{nc}) \cdot T_s}. \tag{6}$$

It turns out the modulator gains seen by the fast loop and slow loop have the same magnitude but are different in sign. Therefore, a unified modulator gain F_m is used in the model of

Fig. 4, which is the same as (6)

$$F_m = \frac{\hat{d}}{\langle \widehat{V}_i \rangle} = \frac{2}{(S_n - S_{nc}) \cdot T_s}. \tag{7}$$

As a common problem of multiple-loop control methods like PCM [13] and V^2 control [14], I^2 ACM control also suffers from "subharmonic oscillation" [15] when the duty ratio is close to or greater than 0.5. An artificial slope can be used to decrease the modulator gain to stabilize the current loop. If a ramp of slope $S_{\rm e}$ is needed, then (7) becomes

$$F_m = \frac{\hat{d}}{\langle \widehat{V}_i \rangle} = \frac{2}{(S_n - S_{nc} + S_e) \cdot T_s}. \tag{8}$$

If slope compensation is added through a voltage divider, the dividing ratio should also be applied to the current sense resistor of the fast loop which makes it different from that of the slow loop.

B. Sampling Gain

I^2 ACM control uses the ripple of the inductor current in the same way as PCM in the fast loop. The current loop for PCM operates as a sampling system instead of averaged state feedback. By the same derivation process in [3], the fast loop of I^2 ACM control turns out to have the same sampling gain

$$H_e(s) \approx 1 + \frac{s}{\omega_n Q_z} + \frac{s^2}{\omega_n^2} \tag{9}$$

where $Q_z = \frac{-2}{\pi}$, and $\omega_n = \frac{\pi}{T_s}$.

The phenomenon, "subharmonic oscillation," is mainly due to (9), which has two RHP zeroes at half of the switching frequency. Note that this model is only accurate up to half the switching frequency due to approximations. It should be mentioned that (9) is an approximation valid only for constant frequency operation. However, in variable frequency operation like constant on-time control, (9) fails to describe the sampling effect [16].

Due to the PI controller in the slow loop, the output contains the average signal for the inductor current; therefore, the slow loop is true state feedback [17] and the sampling gain from (9) is not shown in the slow loop as depicted in Fig. 4.

C. Feedback and Feed-Forward Gain

The feed-forward gain from the input voltage to the inductor current and the feedback gain from the output voltage to the inductor current were fully developed in [3], which is based on a simplified current cell common to all converters. The corresponding derived gains are shown as follows:

$$K'_{f\_fl} = -\frac{DT_sR_i}{L}\left(1 - \frac{D}{2}\right) \tag{10}$$

$$K'_{r\_fl} = \frac{D'^2T_sR_i}{2L} \tag{11}$$

where K'_{f_fl} is the feed-forward gain and K'_{r_fl} is the feedback gain for the invariant current cell in PCM. For different converter topologies, the corresponding feed-forward gain and feedback gain are the combination of (10) and (11) and related to the existence of the input and output voltage during the switch turn-on and turn-off interval.

Since the fast loop in the I^2 ACM control works on the same principle of PCM, the input and output voltages have the equivalent effect on the inductor current through the fast loop.

Although there is a current compensator in the slow loop, the inductor current ripple still appears at the output, because a PI controller is used which has less damping than that of a type II compensator. The feed-forward and feedback effect in the slow loop will be modified by the current compensator as shown in

$$K'_{f\_sl} = K'_{f\_fl} \cdot G_{ci} \tag{12}$$

$$K'_{r\_sl} = K'_{r\_fl} \cdot G_{ci}. \tag{13}$$

As discussed in the modulator gain section, a PI controller contributes a phase delay close to 180°, which can be approximated as an inverted input signal with magnitude magnification at the switching frequency

$$K'_{f\_sl} = K'_{f\_sl} \cdot |G_{ci}|_{f=f_s} \tag{14}$$

$$K'_{r\_sl} = K'_{r\_fl} \cdot |G_{ci}|_{f=f_s}. \tag{15}$$

Based on (12)–(15), the total feed-forward and feedback gains in I^2 ACM control are

$$\begin{aligned} K'_f &= K'_{f\_fl} + K'_{fsl} \\ &= \left(1 + |G_{ci}|_{f=f_s}\right) \cdot \left[-\frac{DT_sR_i}{L}\left(1 - \frac{D}{2}\right)\right] \end{aligned} \tag{16}$$

$$K'_r = K'_{r\_fl} + K'_{r\_sl} = (1 + |G_{ci}|_{f=f_s}) \cdot \frac{D'^2T_sR_i}{2L}. \tag{17}$$

As stated in [3], the expressions of (16) and (17) are derived from the invariant current cell. The gains K'_f and K'_r are the effects on the inductor current from on-time voltage and off-time voltage across the inductor, respectively. Since the on-time voltage and off-time voltage are linear combinations of the input voltage and the output voltage, the feedforward gain K_f from the input voltage and feedback gain K_r from output voltage can be also represented as linear combinations of K'_f and K'_r. Take the buck converter as an example, the on-time voltage is $V_g - V_o$, the input voltage V_g and output voltage $-V_o$ affects the inductor current through the transfer function K'_f. The off-time voltage is V_o, which affects the inductor current through the gain K'_r. As a result, the feedforward gain K_f from the input voltage is K'_f, and the feedback gain K_r from the output voltage is $-K'_f + K'_r$. The feedforward gain and feedback gain in terms of K'_f and K'_r for three basic dc–dc converters are collected in Table I.

IV. Transfer Function Characteristics

The small-signal model developed in the previous section introduces insight into the advantages of I^2 ACM control. To illustrate the characteristics of fast dynamics and accuracy, the I^2 ACM control is compared with traditional ACM control and PCM control.

TABLE I
FEEDFORWARD GAIN AND FEEDBACK GAIN AS AN REPRESENTATION OF K_f' AND K_r'

	Buck	Boost	Buck–Boost
K_f	K_f'	$K_f' - K_r'$	K_f'
K_r	$-K_f' + K_r'$	K_r'	K_r'

TABLE II
CIRCUIT PARAMETERS FOR THE PROTOTYPE CONVERTER

Para.	Value	Para.	Value	Para.	Value	Para.	Value
V_g	5 V	V_o (V)	3 V	T_s	10 μs	f_s	100 kHz
L	20.78 μH	R_L	0.353 Ω	C	318 μF	R_c	0.169 Ω
R_s	0.065 Ω	Acl	10	$R_i = R_s^* Acl$	0.65 Ω	R	2.8 Ω
S_e	0.1 V/μs	Fm_av	1/1.8	iso_gain	1/3	R_1	15 kΩ
R_2	15 kΩ	C_1	5500 pF				

A buck converter was used to perform this comparison. The frequency responses of the control-to-output voltage, the current loop, audio-susceptibility, and the output impedance were checked. Stability analysis was also performed. The circuit parameters for the converter prototype are collected in Table II. The prototype used here is to investigate the characteristics of I^2 ACM control and is not designed for any specific application nor representative of a typical commercial switch-mode power supply. In Table II, R_s is the resistor inserted in series with the inductor to sample the current, Acl is the current sense gain, R_i is the equivalent sense resistor in the model and R_l is the equivalent resistance of the inductor.

Since the steady-state duty ratio is greater than 0.5, a slope compensation Se is added into the modulation in I^2 control and PCM. This value is used throughout this section except for Figs. 11 and 12. The modulator gain used for ACM is Fm_av, which is a common value for most PWM control chips. The iso_gain indicates the dividing ratio from the current controller to the comparator, which can be multiplied into (1) or (8). The parameters R_1, R_2, and C_1 are the components used to form the current controller in Fig. 5, and are used for both I^2 control and ACM.

A. Current Loop Gain

The current loop gain is the transfer function with the voltage loop open and can be expressed by the following for I^2 control:

$$T_{ii} = G_{id} \cdot F_m \cdot R_i(G_{ci} + H_e). \tag{18}$$

The transfer function is compared with that of PCM and ACM in Fig. 7. With the voltage loop open, I^2 control and ACM behave as an ideal current source at low frequencies. In comparison, PCM has much less low frequency gain which results in dc current error. It is shown that I^2 ACM control increases both the current loop gain and the phase margin. As a result, I^2 control has both fast tracking speed and little overshoot.

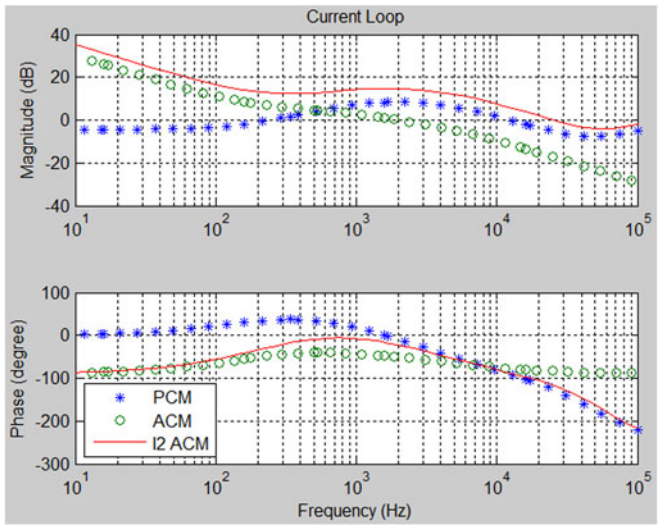

Fig. 7. Current loop transfer functions.

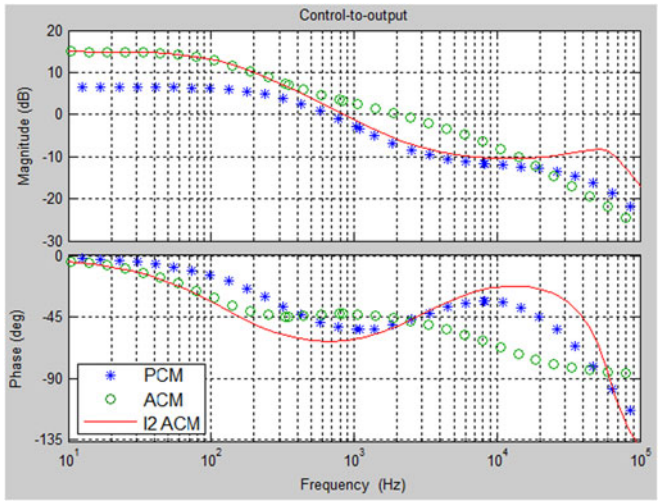

Fig. 8. Control-to-output transfer functions.

B. Control-to-Output Voltage

When the voltage loop is closed, the transfer function from the voltage controller output-to-output voltage for I^2 control can be calculated by Mason's gain rule from Fig. 4

$$G_{vc} = \frac{(1 + G_{ci}) \cdot F_m \cdot G_{vd}}{1 + T_{ii} - K_r \cdot F_m \cdot G_{vd}}. \tag{19}$$

Fig. 8 shows a comparison of the three current control methods. As can be seen, I^2 control behaves like ACM in the low frequency range and PCM in the mid-range frequency. The peaking at half of the switching frequency indicates a pair of double poles which needs to be damped by an artificial ramp.

C. Audio Susceptibility

The closed-loop audio susceptibility is defined as the transfer function of the input-to-output voltage with closed current loops and an open voltage loop. Because of the different frequency responses of the current loops for I^2 ACM control, PCM and

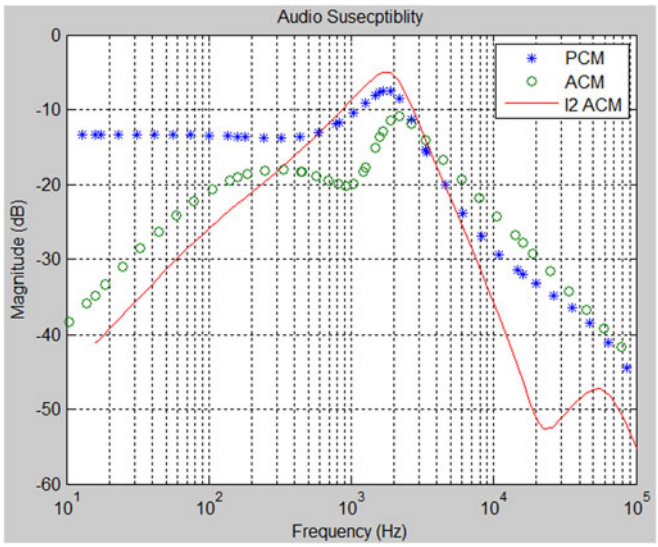

Fig. 9. Comparison of audio susceptibility.

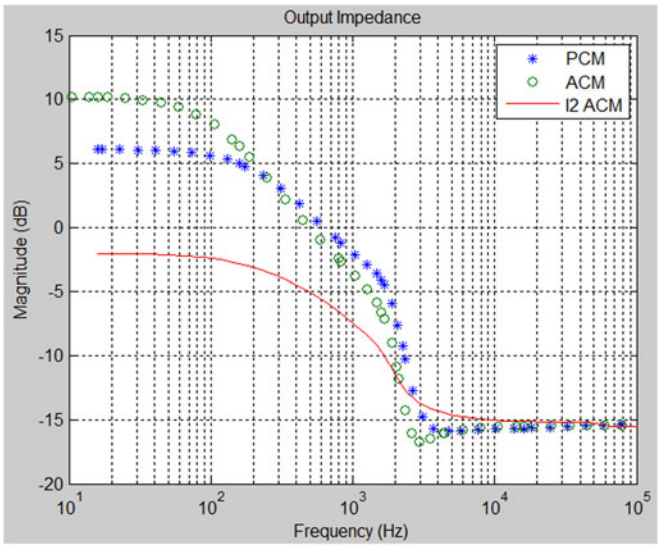

Fig. 10. Comparison of output impedance.

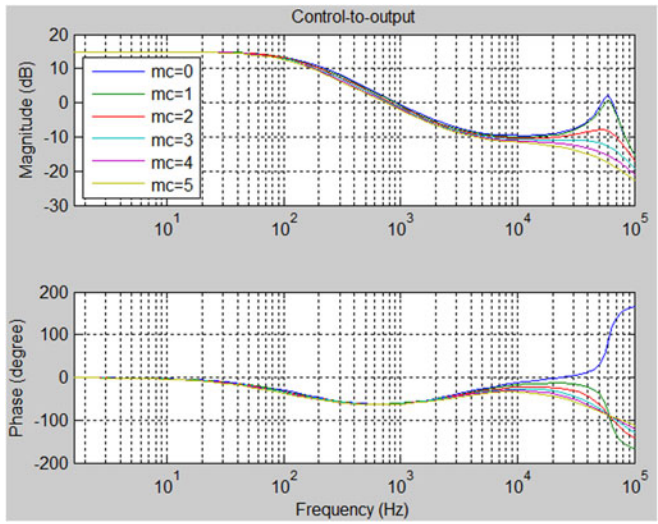

Fig. 11. Control-to-output voltage for different m_c for a 3 V output.

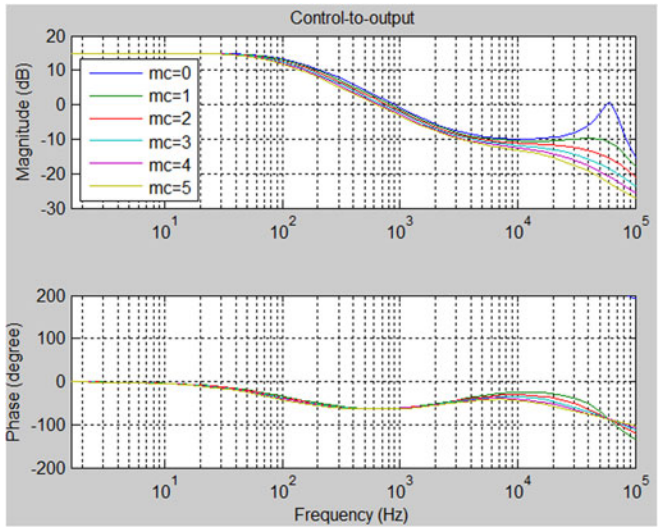

Fig. 12. Control-to-output voltage for different m_c for a 2 V output.

ACM, the effect of the voltage loop compensators are ignored to reveal the effect of the current loops. The audio-susceptibility of I^2 ACM control can be solved by a set of equations [18] developed from Fig. 4. Due to the open voltage loop, the current command $\widehat{I}_c$ is zero here

$$\begin{aligned}\widehat{V}_o &= \widehat{V}_g G_{vg} + \hat{\mathrm{d}} G_{vd} - \widehat{I}_o Z_{\mathrm{out}} \\ \hat{\mathrm{d}} &= F_m[\widehat{V}_g k_f + \widehat{V}_o k_r - \widehat{I}_L (H_e + G_{ci}) R_i] \\ \widehat{I}_L &= \widehat{V}_g G_{ig} + \hat{d} G_{id} + \widehat{I}_o G_{iL}. \end{aligned} \tag{20}$$

For the derivation of the audio-susceptibility transfer function, the output current is assumed to be constant. Therefore, the small-signal variable $\widehat{I}_o = 0$. The resulting transfer function is

$$\frac{\widehat{V}_o}{\widehat{V}_g} = \frac{G_{vg}\,(1 + T_{ii}) + F_m \cdot G_{vd}[K_f - G_{ig}\,(H_e + G_{ci})\,R_i]}{1 + T_{ii} - K_r \cdot F_m \cdot G_{vd}}. \tag{21}$$

The comparison of the audio-susceptibilities under these control techniques is shown in Fig. 9. It is obvious that the audio-susceptibility is improved significantly with I^2 control, which has the lowest magnitude in the low frequency range. PCM is the most sensitive control method in this case because of the higher magnitude at low frequencies. To include the effect of the voltage loop compensator, which is not discussed here, the variation from the voltage loop can be written into the duty ratio expression in (20), and the desired transfer function can be derived.

D. Output Impedance

The output impedance indicates the output voltage drop during load change, which is also modified by the control method. To reveal the characteristics of I^2 control in this comparison, the output impedance developed here is calculated with the current

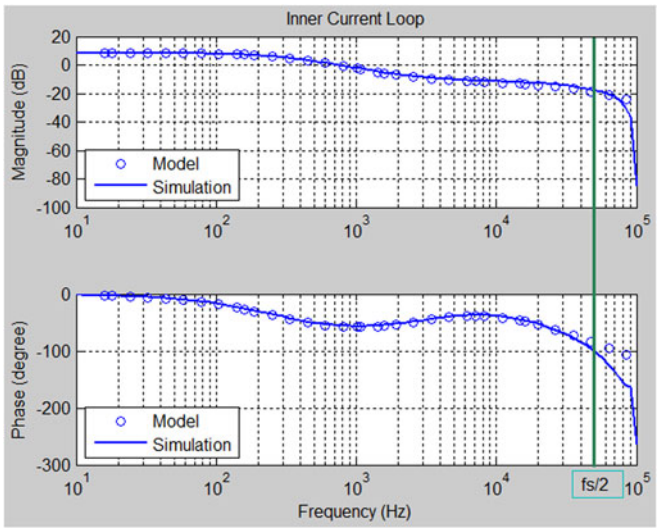

Fig. 13. Model prediction and simulation result of (24) with 5 V input.

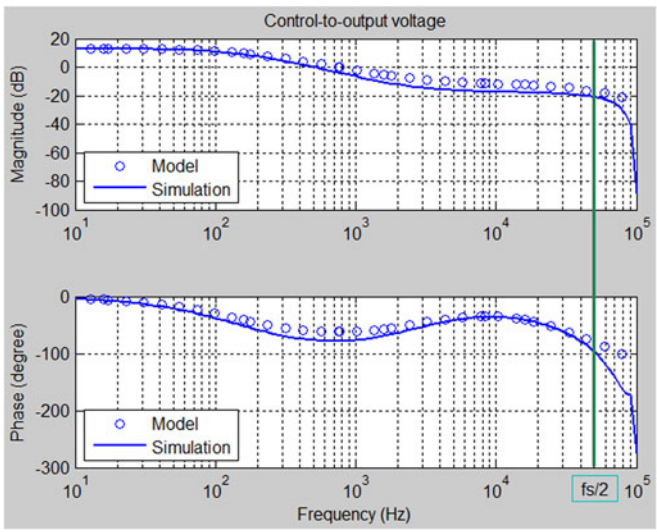

Fig. 14. Model prediction and simulation result of (19) with 5 V input.

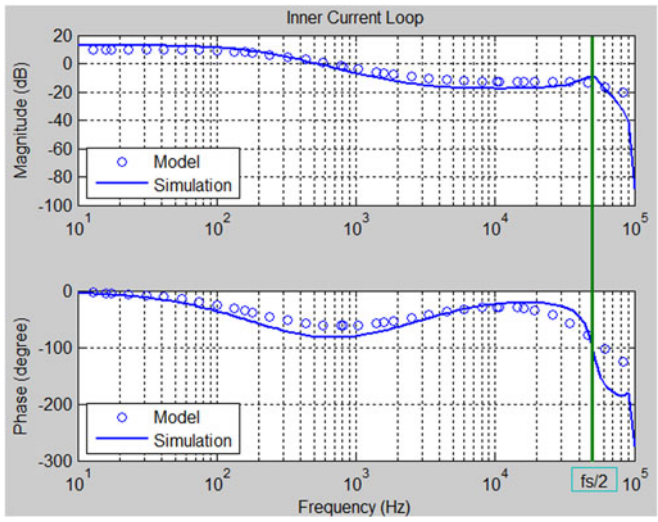

Fig. 15. Model prediction and simulation result of (24) with 6 V input.

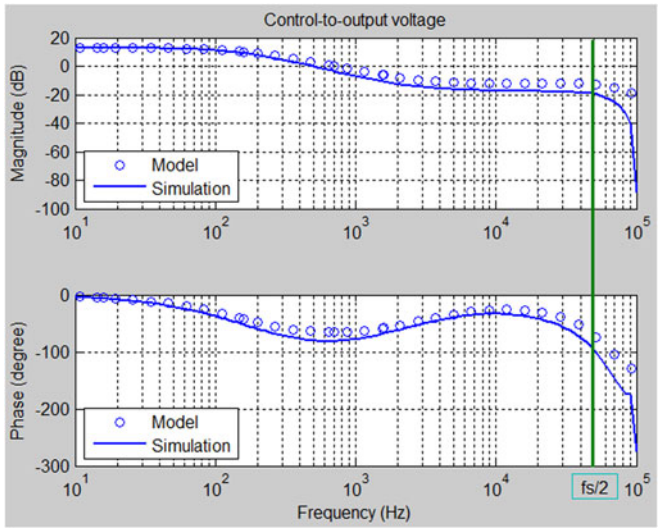

Fig. 16. Model prediction and simulation result of (19) with 6 V input.

loops closed and the voltage loop open; thus, the voltage compensator is ignored here. Using the set of (20) and with the variable $\widehat{V}_g = 0$, the output impedance can be represented as

$$\frac{\widehat{V}_o}{-\widehat{I}_0} = \frac{Z_{\text{out}}\,(1+T_{ii}) + G_{vd}F_m G_{iL}(H_e+G_{ci})R_i}{1+T_{ii}-K_r\cdot F_m\cdot G_{vd}}. \quad (22)$$

It can be seen in Fig. 10 that the output impedance for the three control methods has similar curvature and almost the same values above half of the switching frequency. Since the current loops have fairly low gain at high frequency, the characteristics of the power stage output impedance will be the dominant factor. Below half of the switching frequency, I^2 ACM has the lowest output impedance, which makes it an excellent solution for applications having frequent load change.

However, the voltage loop is always closed in the real applications. In this circumstance, the output impedance for I^2 control is modified by the voltage loop compensator G_c

$$Z_{\text{out\_cl}} = \frac{Z_{\text{out}}\,(1+T_{ii}) + G_{vd}F_m G_{iL}(H_e+G_{ci})R_i}{1+T_{ii}-F_m G_{vd}[K_r+G_c\,(1+G_{ci})]}.$$

E. Stability

It is of great interest to know whether I^2 control is stable and if slope compensation is needed. Adding an external slope decreases the loop gain, reduces the bandwidth, and slows down the transient speed. Let us define a parameter

$$m_c = \frac{S_e}{S_n}. \quad (23)$$

Fig. 11 shows the control-to-output voltage transfer function with m_c as a variable. When $m_c = 0$, the magnitude peak and phase increase at half of the switching frequency indicating a pair of right half-plane poles, which is the reason for the system

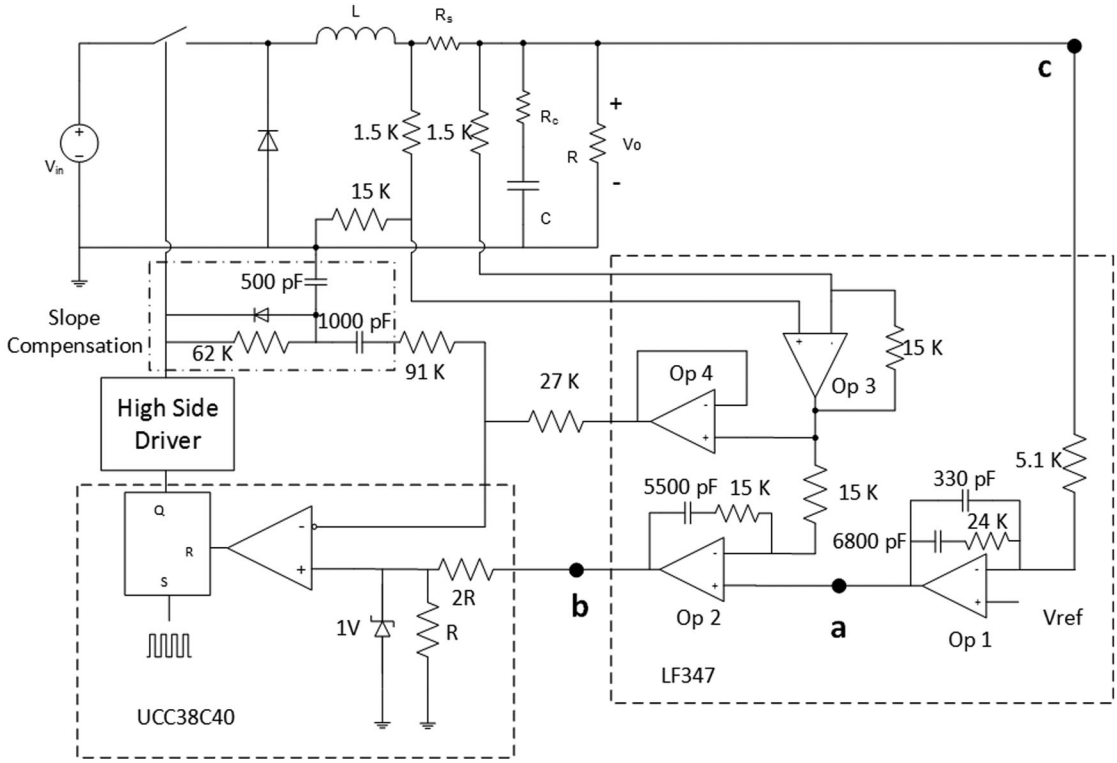

Fig. 17. Schematic of the buck converter prototype.

being unstable. For I^2 ACM control, the control loop still suffers oscillation without slope compensation even when the duty ratio is down to 0.4. Fig. 12 shows the results when the nominal output voltage was decreased to 2 V. The magnitude peak at half the switching frequency goes through 0 dB and causes a second crossover as commonly seen in PCM. This same phenomenon happens when $m_c = 1$ in Fig. 11. Slope compensation can help dampen this peaking and move the RHP poles into the left half plane.

V. Simulation and Experimental Verification

The same buck converter with a 2 V output in Section IV was used as an example to compare the frequency response of the model as plotted with MATLAB versus simulation results from Simplis and measurements using an AP300 network analyzer from Ridley Engineering. With a 5 V input and a 2 V output, the circuit still suffered from the subharmonic oscillation as illustrated in Fig. 12. Therefore, the input voltage was selected to vary from 3.3 to 6 V, and the steady-state duty cycle varies from 0.33 to 0.606.

A. Simulation Results

The first simulation was performed to verify the validation of the fast loop model shown in Fig. 13, in which both the voltage loop and the slow current loop were open. Instead of measuring inductor current response due to the perturbation in control signal $\widehat{V}_i$, the response on the output voltage is measured. The corresponding transfer function is given as

$$G_{i\_fl} = \frac{F_m \cdot G_{vd}}{1 + T_i - K_{r\_fl} \cdot F_m \cdot G_{vd}} \tag{24}$$

where $T_i = F_m \cdot G_{id} \cdot R_i \cdot H_e$ is the open-loop transfer function of the most inner current loop. Since the slow loop is open, the feedback gain K_{r_sl} is not taken into consideration. With only the fast loop closed, the circuit behaves in the same way as PCM which determines the duty ratio using only the slope of the inductor current. Therefore, (24) is the same as the control-to-output transfer function for PCM. As seen from Figs. 13 and 15, the model prediction matches very well with the simulation results from Simplis.

The second test was to verify the accuracy of (19) with $S_e = 0.75$ V/T$_s$, which is illustrated in Fig. 14. The difference in the mid-range is mainly due to the nonideal operational amplifier of the current controller used in the simulations [9]. The reason behind picking (19) and (24) is that these two transfer functions can be measured with a network analyzer; therefore, the simulation results can be verified with measurements. With the model confirmation of the I^2 control operating with slope compensation, it is also of interest to check the control technique without the external slope. To stabilize the circuit without the help of slope compensation, the input voltage was increased to 6 V to decrease the duty ratio. The same comparison between the model prediction and simulation results is shown in Figs. 15 and 16.

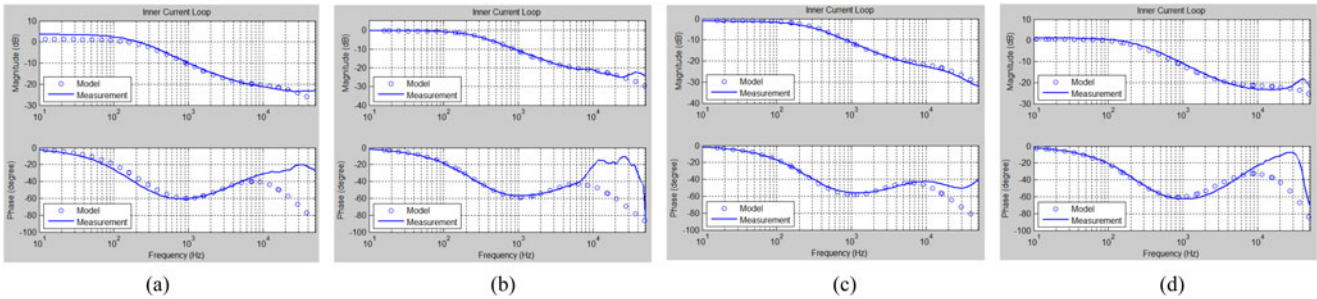

Fig. 18. Measurement of closed inner current loop with input voltage: (a) 3.3 V, (b) 5 V, (c) 6 V, and (d) 6 V without slope.

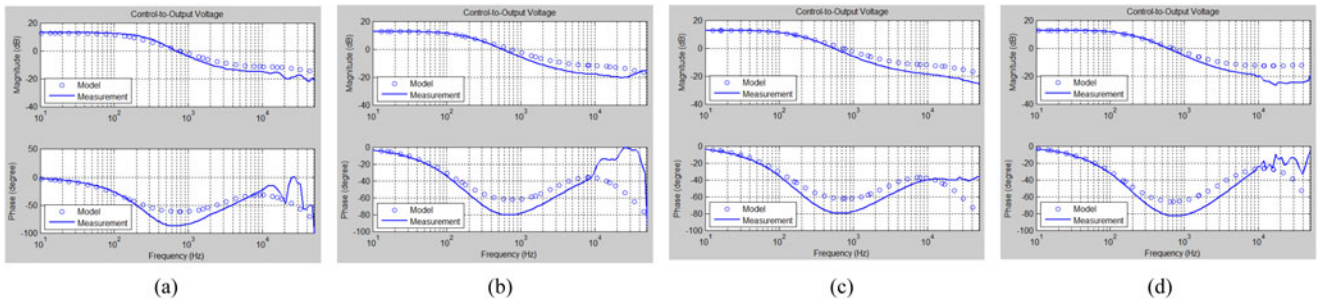

Fig. 19. Measurement of control-to-output voltage with input voltage: (a) 3.3 V, (b) 5 V, (c) 6 V, and (d) 6 V without slope compensation.

B. Experimental Results

To further verify the modeling discussed, a prototype buck converter was constructed using a TI UCC38C40 and an LF347 quad operational amplifier. The schematic of the overall system is shown in Fig. 17. Since there are three control loops, the voltage loop and slow loop were implemented using op amps 1 and 2 of the LF347, respectively. Op amp 3 was programmed as a current sense amplifier with gain of 10. Finally, op amp 4 was connected as a voltage follower and utilized in the slope compensation circuit. The slope compensation is generated from the switch gate driver signal [19], which maintains circuit operation in the constant frequency mode. The slope compensated inductor current signal was fed into the negative input of the comparator on the UCC38C40. It should be noted that there is a gain of 1/3 between the comp pin and the positive input of the comparator. Thus, the output of op amp 2 was scaled and compared with the inductor current peak signal. The voltage compensator was designed using the K factor method [20] based on the frequency response of (19).

The frequency responses were measured using the AP300 network analyzer. To measure the transfer function of (24), the voltage loop and slow loop were open, a voltage source is connected at point b to provide the dc-bias voltage. The responses are collected in Fig. 18. The measurements from point a to point c in Fig. 19 corresponds to the results of (19).

In experimental tests, the input voltage was selected as 3.3, 5, and 6 V as shown in Figs. 18 and 19. For the 6 V input, the frequency response was measured with and without slope compensation. Since the signal beyond half of the switching frequency was noisy and distorted, the comparison of the model and measurement was conducted in the range from 10 Hz to half of the switching frequency. As can be seen from Figs. 18 and 19, the proposed model matches the measurement very well. It should be noted that the magnitude dip in Fig. 19 is smaller than 2 dB, which was also reported in [7].

VI. Conclusion

I^2 ACM control is a promising technique which provides the advantages of fast dynamic speed and precise current control. The current loop uses the both the average current signal and the peak current value to determine the PWM output; therefore, an ideal current source with cycle-by-cycle current limiting is achieved.

Because of the existence of three control loops, the analysis of I^2 ACM control is more complicated than the traditional current mode control methods. In this paper, I^2 ACM control is taken as a combination of average current control and peak current control and analyzed loop by loop. The small-signal characteristics of such control technique were compared with ACM and PCM, which revealed the advantages of I^2 control. The large low-frequency gain and bandwidth confirm that I^2 ACM control is fast and accurate. The complex poles at half of the switching frequency will move into the right half-plane when the duty ratio is close to or greater than 0.5. The resonant peak produced by these poles would cause a second crossover even with duty ratio down to 0.4. An external slope can be added to the sensed inductor peak current to move the poles into the left half-plane and damp the resonant peak.

The model proposed in this paper for I^2 ACM control was confirmed with simulation results from Simplis and measurements

with an AP300 network analyzer. The frequency responses predicted by the proposed model for the inner current loop and control-to-output voltage matched those obtained from simulation and measurements. As a result, the proposed model is useful in the design of the current loop and voltage loop compensators for I^2 ACM controllers operating at constant switching frequency.

REFERENCES

[1] C. W. Deisch, "Simple switching control method changes power converter into a current source," in *Proc. Power Electron. Spec. Conf.*, 1978, vol. 1, pp. 300–306.

[2] R. D. Middlebrook, "Topics in multiple-loop regulators and current-mode programming," *IEEE Trans. Power Electron.*, vol. PE-2, no. 2, pp. 109–124, Apr. 1987.

[3] R. B. Ridley, "A new small-signal model for current-mode control," Ph.D. dissertation, Bradly Dept. Elect. Computer Eng., Virginia Polytechnic Inst. State Univ., Blacksburg, VA, USA, 1990.

[4] F. D. Tan, "Modeling and control of switching converters: I. Unified modeling and measurement of current-programmed converters. II. A generic averaged model for switches in dc-to-dc converters," Ph.D. dissertation, Dept. Elect. Eng., California Inst. Technol., Pasadena, CA, USA, 1994.

[5] L. Dixon, "Average current mode control of switching power supplies," in *Proc. Unitrode Power Supply Design Seminar Manual SEM700*, 1990, pp. 1–12.

[6] P. Cooke, "Modeling average current mode control," in *Proc. IEEE Appl. Power Electron. Conf. Expo.*, 2000, vol. 1, pp. 256–262.

[7] W. Tang, "Average current mode control and charge control for PWM converters," Ph.D. dissertation, Bradly Dept. Elect. Computer Eng., Virginia Polytechnic Inst. State Univ., Blacksburg, VA, USA, 1994.

[8] F. Yu, F. C. Lee, and P. Mattavelli, "A small signal model for average current mode control based on describing function approach," in *Proc. IEEE Energy Convers. Cong. Expo.*, 2011, pp. 405–412.

[9] Y. Yan, F. C. Lee, P. Mattavelli, and P.-H. Liu, "I^2 average current mode control for switching converters," in *Proc. IEEE Appl. Power Electron. Conf. Expo.*, 2013, pp. 229–236.

[10] S. Qu, "Modeling and design considerations of V^2 controlled buck regulator," in *Proc. IEEE Appl. Power Electron. Conf. Expo.*, 2001, vol. 1, pp. 507–513.

[11] V. Vorpérian, "Simplified analysis of PWM converters using model of PWM switch. I. Continuous conduction mode," *IEEE Trans. Aerosp. Electron. Syst.*, vol. 26, no. 3, pp. 490–496, May 1990.

[12] R. W. Erickson and D. Maksimovic, *Fundamentals of Power Electronics*. New York, NY, USA: Springer, 2001.

[13] Y. Yingyi, F. C. Lee, and P. Mattavelli, "Analysis and design of average current mode control using describing function-based equivalent circuit model," in *Proc. IEEE Energy Convers. Congr. Expo.*, 2012, pp. 2237–2244.

[14] J. Sun, "Characterization and performance comparison of ripple-based control for voltage regulator modules," *IEEE Trans. Power Electron.*, vol. 21, no. 2, pp. 346–353, Mar. 2006.

[15] C. C. Fang, "Unified subharmonic oscillation conditions for peak or average current mode control," *Int. J. Circuit Theory Appl.*, 2014.

[16] J. Li and C. L. Fred , "New modeling approach and equivalent circuit representation for current-mode control," *IEEE Trans. Power Electron.*, vol. 25, no. 5, pp. 1218–1230, May 2010.

[17] J. Sun and R. M. Bass, "Modeling and practical design issues for average current control," in *Proc. IEEE Appl. Power Electron. Conf. Expo.*, 1999, vol. 2, pp. 980–986.

[18] R. Ahmadi and M. Ferdowsi, "Modeling closed-loop input and output impedances of DC-DC power converters operating inside DC distribution systems," in *Proc. IEEE Appl. Power Electron. Conf. Expo.*, 2014, pp. 1131–1138.

[19] C. Basso, "Ramp compensation for current-mode converters," *Power Electronics*, 2004.

[20] H. D. Venable, "The K factor: A new mathematical tool for stability analysis and synthesis," in *Proc. Powercon*, 1983, vol. 10, pp. H1–1.

Siyu He (S'11) received the B.S. degree in electrical engineering from Central South University, Changsha, China, in 2011. Concentrating in power electronics, he received the Ph.D. degree from the Department of Electrical and Computer Engineering, Auburn University, Auburn, Al, USA, in 2015.

He is currently with the Delta Electronics, Taipei, Taiwan. His research interests are in digital control of switching power converters, including modeling, design, simulation, and DSP implementation.

John Y. Hung (S'79–M'80–SM'93–F'11) received the B.S. degree from the University of Tennessee, Knoxville, TN, USA, the M.S.E. degree from Princeton University, Princeton, NJ, USA, and the Ph.D. degree from the University of Illinois, Urbana-Champaign, Champaign, IL, USA, in 1979, 1981, and 1989, respectively, all in electrical engineering.

From 1981 to 1985, he was with Johnson Controls, Milwaukee, WI, developing microprocessor-based controllers for commercial heating, ventilation, and air conditioning systems. From 1985 to 1989, he was a Consultant Engineer with PolyAnalytics, Inc. In 1989, he joined Auburn University, Auburn, AL, USA, where he is currently a Professor of electrical and computer engineering. His teaching and research interests include nonlinear control systems and signal processing with applications in process control, robotics, electric machinery, and power electronics.

Dr. Hung has received several awards for his teaching and research, including a Best Paper Award for the IEEE TRANSACTIONS ON INDUSTRIAL ELECTRONICS, and two U.S. patents in the area of control systems. He served as an Associate Editor of the IEEE TRANSACTIONS ON CONTROL SYSTEM TECHNOLOGY (1997, 1998), and the IEEE TRANSACTIONS ON INDUSTRIAL ELECTRONICS (1996–2005). He was also the President of the IEEE Industrial Electronics Society (2014, 2015).

R. M. Nelms (F'04) received the B.E.E. and M.S. degrees in electrical engineering from Auburn University, Auburn, AL, USA, in 1980 and 1982, respectively, and the Ph.D. degree in electrical engineering from Virginia Polytechnic Institute and State University, Blacksburg, VA, USA, in 1987.

He is currently Professor and Chair of the Department of Electrical and Computer Engineering, Auburn University. His research interests are in power electronics, power systems, and electric machinery.

Dr. Nelms is a registered Professional Engineer in Alabama. In 2004, he was named an IEEE Fellow "for technical leadership and contributions to applied power electronics."